Chinese Chemical Letters 37 (2026) 112209

Contents lists available at ScienceDirect

Chinese Chemical Letters

journal homepage: www.elsevier.com/locate/cclet

Treatment of nitrogen-contained refractory organic wastewater by micron zero-valent iron based two-stage process: Synergistic contaminant degradation and ammonia nitrogen formation

Yan Zhang[a,b], Shuo Chen[a,b], Huihui Peng[a,b,c], Ankang Wang[a,b], Yiming Sun[a,b], Chenying Zhou[a,b], Shuang Meng[a,b], Chuanshu He[a,b], Peng Zhou[a,b,*], Bo Lai[a,b,*]

[a] State Key Laboratory of Hydraulics and Mountain River Engineering, College of Architecture and Environment, Sichuan University, Chengdu 610065, China
[b] Sino-German Centre for Water and Health Research, Sichuan University, Chengdu 610041, China
[c] College of Environmental Science, Sichuan Agricultural University, Chengdu 611130, China

ARTICLE INFO

Article history:
Received 2 October 2025
Revised 1 December 2025
Accepted 2 December 2025
Available online 4 December 2025

Keywords:
Microscale zero-valent iron
Nitrogen transformation
Refractory organic wastewater
Ammonia nitrogen formation
Two-stage gradient oxidation process

ABSTRACT

The treatment of nitrogen-contained refractory organic wastewater faces challenges due to complex composition and high toxicity. While microscale zero-valent iron (mZVI) based processes enable simultaneous removal of organic contaminants and nitrate (NO_3^--N), electron competition and excessive iron sludge generation limit efficiency. This study reveals the dual roles of NO_3^--N in the mZVI/O_2 process: Inhibiting the oxidative removal of organic contaminants through electron competition and simultaneously enhancing iron dissolution with T_{Fe} increased by 17.5 % to 65.7 % compared to the system without NO_3^--N. Nitrogen conversion analysis indicates that NO_3^--N is mainly converted to NH_4^+-N *via* a direct 8-electron reduction pathway. To increase the utilization efficiency of iron electrons and enhance organic contaminant removal, a two-stage gradient oxidation process (mZVI/O_2-Fenton) is designed: 1st stage utilizes NO_3^--N to enhance Fe^0 corrosion for NO_3^--N reduction and Fe(II) release, while 2nd stage achieves efficient organic contaminants degradation *via* Fenton reaction with addition of H_2O_2. Actual wastewater validation confirms synergistic high organic contaminants removal (COD removal > 79.5 %) and targeted nitrogen conversion (>66.4 % NO_3^--N to NH_4^+-N). The study overcomes electron competition limitations in the mZVI/O_2 process and provides a synergistic pollution control-resource recovery strategy for NO_3^--N-contained refractory organic wastewaters.

© 2026 Published by Elsevier B.V. on behalf of Chinese Chemical Society and Institute of Materia Medica, Chinese Academy of Medical Sciences.

Nitrogen-contained refractory organic wastewater is mainly derived from industrial activities including chemical manufacturing, pharmaceutical production, and textile dyeing. These wastewaters frequently contain inorganic nitrogen (*e.g.*, nitrate (NO_3^--N) and ammonium (NH_4^+-N)) and refractory organic contaminants (*e.g.*, phenolic compounds, heterocyclic compounds, and polycyclic aromatic hydrocarbons), conferring high organic load, complexity, toxicity, and resistance to degradation. Conventional biological processes, which rely on microbial nitrogen conversion, are largely ineffective against such refractory contaminants [1]. Synergistic bottlenecks between nitrogen transformation and organic contaminant degradation (*e.g.*, electron donor competition and inhibition by intermediates) further amplify treatment challenges [2]. Meanwhile, ammonia (NH_3) can be recovered as high-value products (*e.g.*, struvite and ammonium sulfate) *via* adsorption or ion exchange for agricultural and industrial applications [3]. Existing technologies are unable to synergistically achieve contaminant mineralization and targeted nitrogen transformation (from NO_3^--N to NH_4^+-N) for NH_3 recovery [4]. Therefore, developing integrated technology for simultaneous contaminant degradation and targeted nitrogen transformation is an urgent task for treating nitrogen-contained refractory organic wastewater.

Zero-valent iron (ZVI)-based wastewater treatment processes are effective in treating nitrogen-contained refractory organic wastewaters. As a reactive metal ($E^0 = -0.44$ V), microscale ZVI (mZVI) removes refractory organic contaminants synergistically *via* direct reduction and indirect oxidation. In the direct reduction process, mZVI as the electron donor can release electrons *via* the oxidation of Fe^0 to Fe(II), thereby directly reducing electron-deficient contaminants, including heavy metals [5], NO_3^--N [6], nitroaromatics [7], and chlorinated organic contaminants [8]. Concurrently, hydrogen atoms ($H^•$) generated during mZVI corrosion can also indirectly reduce above organic contaminants [9,10]. In the indi-

* Corresponding authors.
E-mail addresses: zhoup1219@sina.com (P. Zhou), laibo@scu.edu.cn (B. Lai).

https://doi.org/10.1016/j.cclet.2025.112209
1001-8417/© 2026 Published by Elsevier B.V. on behalf of Chinese Chemical Society and Institute of Materia Medica, Chinese Academy of Medical Sciences.

rect oxidation process, mZVI corrosion releases electrons for reducing O_2 *via* two electrons transfer to generate H_2O_2, initiating Fenton reactions to generate hydroxyl radicals ($^{\bullet}OH$) for efficient organic contaminant degradation (Text S1 in Supporting information) [11,12]. Efficiency enhancements involve coupling with oxidants (*e.g.*, H_2O_2 [13] and O_3 [14]), constructing Fe/Cu systems [15], and employing iron-carbon micro-electrolysis systems which utilize the micro-galvanic cells formed by iron and carbon to enhance electron transfer [16]. Currently, mZVI-based processes demonstrate engineering-scale implementation in environmental remediation, enabled by synergistic direct reduction and indirect oxidation pathways.

First employed for NO_3^--N removal in the 1970s [17], ZVI preferentially reduces NO_3^--N into NH_4^+-N (or NH_3) and N_2 *via* direct electron transfer through its surface corrosion layer (Text S2 in Supporting information), releasing Fe(II) [2]. Complete NO_3^--N reduction occurs within hours under acidic conditions [18], dominated by mZVI-surface direct electron transfer [19]. Furthermore, the mZVI-based processes demonstrate efficiently degrade refractory organic contaminants. For instance, the mZVI/O_3 process attains an 89.5 % COD removal rate for *p*-nitrophenol (PNP)-containing wastewater within 60 min [14]. Through synergistic approaches of direct reduction and indirect oxidation, the mZVI-based processes enable simultaneous conversion from NO_3^--N to NH_4^+-N and degradation of refractory organic contaminants, preliminarily validating its feasibility for co-treatment of nitrogen and organic contaminants in nitrogen-contained refractory organic wastewater.

In early studies, researchers focused only on the reaction kinetics of single solute systems, without considering the potential effects of coexisting electron acceptors [2]. As research progressed, it was found that when NO_3^--N coexists with organic contaminants, its high oxidation leads to high-reactivity with ZVI, thereby inhibiting organic contaminants reduction efficiency (*e.g.*, halogenated hydrocarbon dehalogenation) through competitive occupation of reactive sites and electron consumption [20]. While increasing the dosages of ZVI can alleviate competition, it will increase the generation of iron sludge [21]. The sulfur-modified ZVI (S-ZVI) can inhibit the reduction of NO_3^--N but fails to achieve its targeted removal [22]. Additionally, the indirect oxidation in ZVI-based processes relies on ZVI and its corrosion product Fe(II) to release electrons for activating dissolved oxygen/oxidants. Electron competition from NO_3^--N may affect oxidation pathways [2], but there is still a lack of quantitative studies on the suppression of oxidation. Notably, NH_4^+-N as the main reduction product of NO_3^--N in the mZVI/O_2 process may be further oxidized to NO_3^--N by $^{\bullet}OH$ or other reactive oxygen species (ROS) [23], initiating an inorganic nitrogen redox cycle, needlessly consuming iron electrons (Fig. S1 in Supporting information). This cycle not only wastes electrons and generates excessive iron sludge, but also may reduce the overall oxidation efficiency of organic contaminants. To address these challenges, it is necessary to clarify the dynamic coupling mechanism between inorganic nitrogen transformations and redox activities. Therefore, a two-stage gradient oxidation process (mZVI/O_2-Fenton) was proposed to synergize the degradation of organic contaminants and the directed transformation of NO_3^--N to NH_4^+-N. However, the effect of inorganic nitrogen transformations (*e.g.*, NH_4^+-N oxidation) still needs to be further verified.

This study investigates the mechanisms of inorganic nitrogen transformation in the mZVI/O_2 process (Fig. 1a) and develops a two-stage gradient oxidation process (mZVI/O_2-Fenton) (Fig. 1b) for treating high-concentration nitrogen-contained refractory organic wastewater. The inhibition of organic contaminant degradation by inorganic nitrogen in the mZVI/O_2 process was systematically investigated by regulating inorganic nitrogen species, organic contaminant types, and process parameters. The electron competition mechanism of NO_3^--N was elucidated through iron dissolution kinetics and ROS analysis, clarifying NO_3^--N interference on H_2O_2 production and $^{\bullet}OH$ formation. Simultaneously, the morphological and compositional evaluations of mZVI powders were analyzed by scanning electron microscope (SEM), X-ray photoelectron spectroscopy (XPS), and X-ray diffraction (XRD) to explain the regulatory effects of inorganic nitrogen on mZVI corrosion and passivation layer formation. Furthermore, the migration and transformation pathways of inorganic nitrogen in the mZVI/O_2 process were tracked, and the mZVI/O_2-Fenton process was designed by integrating the selective oxidation behavior of NH_4^+-N in Fenton/Fenton-like systems. Finally, the synergistic efficiencies of organic contaminant degradation, NH_4^+-N generation as well as the optimization potential of electron utilization efficiency were validated by treating high-concentration nitrogen-contained refractory organic wastewaters derived from multiple chemical plants.

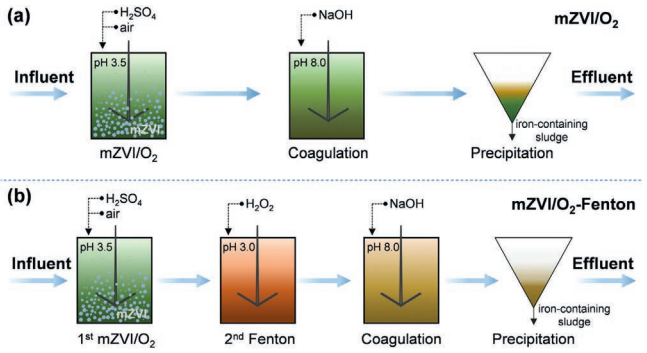


Fig. 1. Process flow diagrams of (a) mZVI/O_2 process and (b) two-stage gradient oxidation process (mZVI/O_2-Fenton).

The details of all chemicals, analysis and characterization methods were provided in Texts S3-S9 in Supporting information.

The effect of inorganic nitrogen species (NO_3^--N, NO_2^--N, and NH_4^+-N) on organic contaminant removal in the mZVI/O_2 process was investigated, with phenol (PE) was selected as the target contaminant. Fig. 2a depicts that high concentrations of NO_3^--N and NO_2^--N can significantly inhibit the mZVI/O_2 process to remove organic contaminants, whereas the effect of NH_4^+-N was unobvious. The distinct oxidation–reduction characteristics of nitrogen species likely underlie this inhibition. Under acidic conditions (pH 3.5), NO_3^--N undergoes preferential reduction on the Fe^0 surface, competing for electrons required for oxidizing organic contaminants [24]. Although the oxidizing capacity of NO_2^--N is weak, it can act as an electron donor and acceptor, thus significantly affecting the redox pathways. The concentration effects (50–200 mg/L) of NO_3^--N were further investigated due to its widespread presence in real wastewater (Fig. 2b). With the increase of NO_3^--N concentration, the removal of COD and TOC significantly decreased, and the k_{obs} for PE removal decreased to less than half of that in the absence of NO_3^--N (Fig. S2 in Supporting information). This inhibitory effect might be associated with the electron competition and surface passivation, which are inherent disadvantages of the mZVI/O_2 process.

The performance of mZVI exhibits a pH-dependent phenomenon, and the main reason is attributed to electron competition and surface passivation. The performance of mZVI/O_2 process greatly depended on pH within the range of pH 2.0–6.0, with the best performance at pH 3.5 (Fig. 2c). The corrosion of mZVI was obviously enhanced with the lowering pH, and active sites were generated to improve the contaminant removal and NO_3^--N reduction, while side reactions would happen when the pH is to too low [25]. Although the pH showed the same changing trend, because NO_3^--N is an electron acceptor, the electrons available for oxidiz-

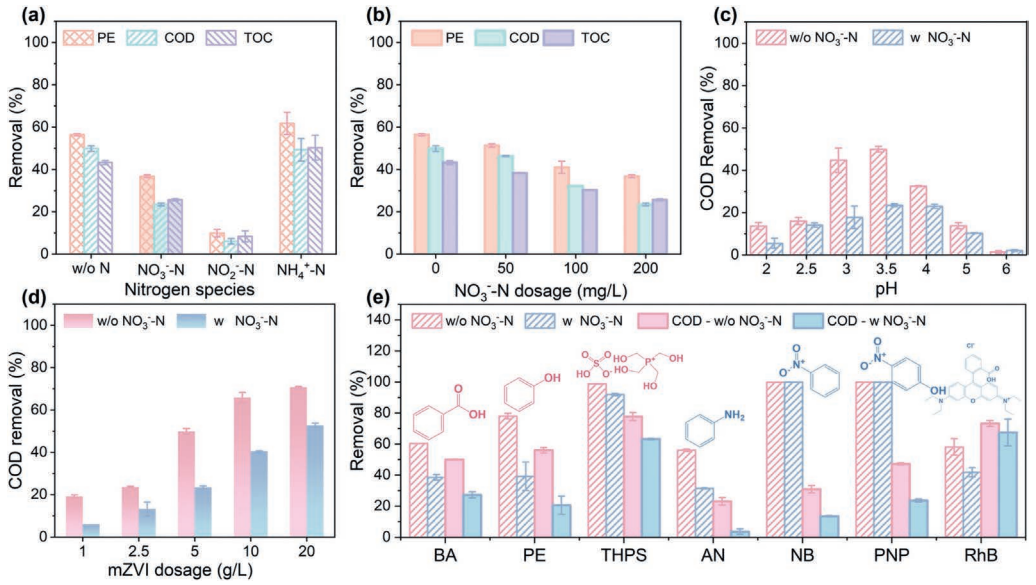


Fig. 2. Effect of (a) nitrogen species, (b) NO_3^--N concentration, (c) pH, (d) mZVI dosage, (e) different organic contaminants on the performance of the mZVI/O_2 process.

ing organic contaminants are decreased, and the overall removal efficiency is always lower than that of the process without NO_3^--N [26]. The increased pH favored the formation of Fe(II)/Fe(III) (oxy)hydroxide passivation layers, and the activity of mZVI was inhibited [11]. The removal efficiency of all systems decreased systematically, regardless of the presence of NO_3^--N. XRD analysis showed that no obvious iron oxide peaks were detected (60 min, pH 3.5), which indicated that NO_3^--N mainly affected the performance by electron competition, and pH mainly affected the mZVI corrosion and active sites formation. Increasing the dosage of mZVI alleviated the inhibitory effect of NO_3^--N by providing more active sites and electrons (Fig. 2d, Figs. S5a and b in Supporting information) [24] and electron competition mechanism was further verified.

In the mZVI/O_2 process, the concentration variation and COD removal of different organic contaminants were significantly different. (Fig. 2e and Fig. S6 in Supporting information). The reduction removal of nitrobenzene (NB) [27] and PNP [14] is not affected by NO_3^--N, which is attributed to the electron-withdrawing capability of -NO_2, enabling NB and PNP to preferentially act as electron acceptors rather than NO_3^--N in the mZVI/O_2 process [28]. However, COD removal was significantly reduced with NO_3^--N. Meanwhile, PE [29], aniline (AN) [27], benzoic acid (BA) [30], tetrakis(hydroxymethyl)phosphonium sulfate (THPS) [31], and rhodamine B (RhB) [32] were removed by indirect oxidation, weak reduction pathways, or flocculation, which significantly decreased their elimination with NO_3^--N. This indicates that NO_3^--N also affects the oxidation of organic pollutants by the mZVI/O_2 process. NO_3^--N may inhibit the Fenton reaction-driven oxidation process by competing with O_2 for abstracting electrons released from mZVI.

It has been reported that NO_3^--N as an iron-reducible anion, curbs the reductive removal of organic contaminants *via* competition for active site or mZVI passivation [26]. This study suggests NO_3^--N further reduces removal efficiency by impairing the indirect oxidation of mZVI through electron competition.

Under aerobic conditions, stepwise oxidation from Fe^0 to Fe(II) and Fe(III) during mZVI corrosion continuously donates electrons driving O_2 reduction to various ROS. The mZVI/O_2 process achieves organic contaminant removal through two main stages: (1) mZVI corrosion generates Fe(II) and releases electrons competitively captured by oxidizing species (O_2, NO_3^--N, and electron-withdrawing groups of organic contaminants); (2) ROS generation *via* Fenton reaction involving Fe(II) and H_2O_2. The whole process is controlled by the rapid escape of iron ions from the mZVI surface [11]. Although NO_3^--N suppresses organic contaminant removal through electron competition, it can also paradoxically enhance mZVI corrosion. To analyze this, the total dissolved iron (T_{Fe}) was determined both with and without nitrogen species (Fig. 3a). NO_3^--N increased T_{Fe} by 25.0 % (from 2.8 g/L to 3.5 g/L), whereas NO_2^--N decreased T_{Fe} by 42.9 % (from 2.8 g/L to 1.6 g/L), with negligible impact from NH_4^+-N. It suggests direct redox interaction of NO_3^--N with mZVI, which promotes the Fe(II) release *via* enhanced corrosion [22]. XPS spectra confirmed NO_3^--N induced greater exposure of reactive Fe^0 sites, accelerating Fe(II) oxidation products generation (Fig. S7 in Supporting information).

In acidic conditions, H^+ and NO_3^--N synergistically accelerate mZVI corrosion, contributing to the maintenance of a high value of T_{Fe}. T_{Fe} can be increased by 17.5 % to 65.7 % with NO_3^--N, which also enhances different organic pollutants removal by mZVI/O_2 (Figs. 3b–d). It increased further with increasing NO_3^--N dosing (Fig. 3e). The standard electrode potential of NO_3^-/NO_2^- (0.01 V) exceeds Fe(II)/Fe^0 (−0.44 V) enabling NO_3^--N to function as a strong electron acceptor that promotes Fe^0 oxidation to Fe(II), enhancing iron dissolution [33]. Under neutral conditions (pH 5.0-6.0), T_{Fe} decreases sharply (pH 6.0, 0.08 g/L with NO_3^--N and 0.03 g/L without NO_3^--N). This stems from Fe(II) and Fe(III) hydrolysis forming dense passivation layers comprising iron (hydroxide)oxides that function as diffusion barriers, inhibiting further iron dissolution (Figs. S4 and S8 in Supporting information). Conversely, NO_3^--N addition increased surface Fe(II) content (Fig. S9 in Supporting information), demonstrating its capacity to continuously drive Fe^0 oxidation even at mild pH, partially counteracting passivation layer inhibition and sustaining mZVI corrosion activity across wide pH ranges.

Increased iron dissolution provides more redox active sites (Fig. 2d and Fig. S10 in Supporting information) [2]. However, although T_{Fe} was consistently higher with NO_3^--N, organic contaminant degradation efficiency was significantly lower. Analysis of COD removal/mZVI consumption ratios (ΔCOD/ΔFe) revealed the ratio was significantly higher without NO_3^--N (Fig. S11 in Supporting information). It indicates that NO_3^--N resulted in a decrease

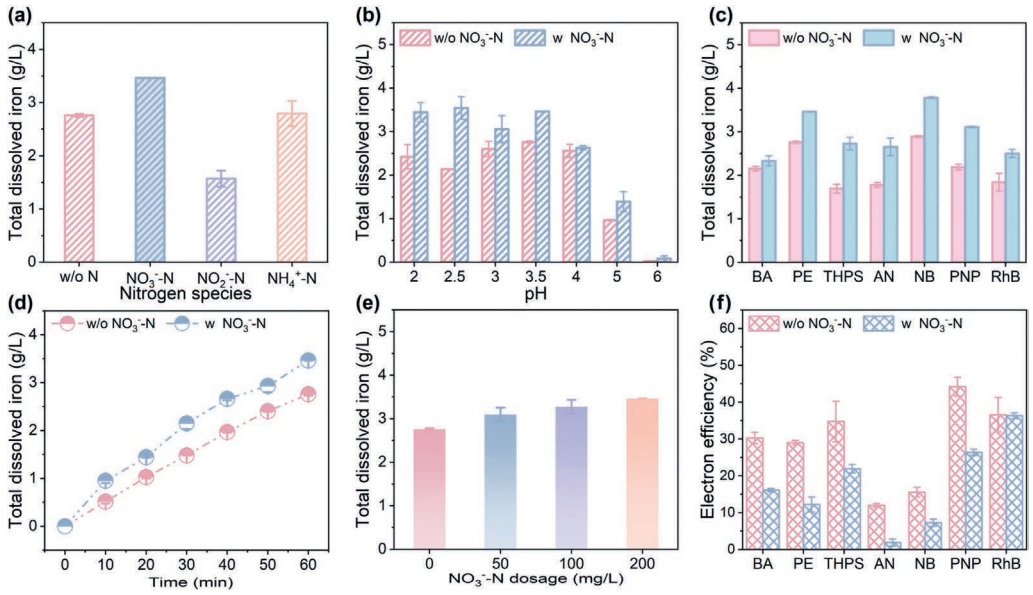


Fig. 3. Total dissolved iron concentration in the reaction solution. Effect of (a) nitrogen species, (b) pH, (c) different organic contaminants, (d) time series data for total dissolved iron, (e) NO_3^--N concentration, (f) iron electron utilization in different organic contaminants.

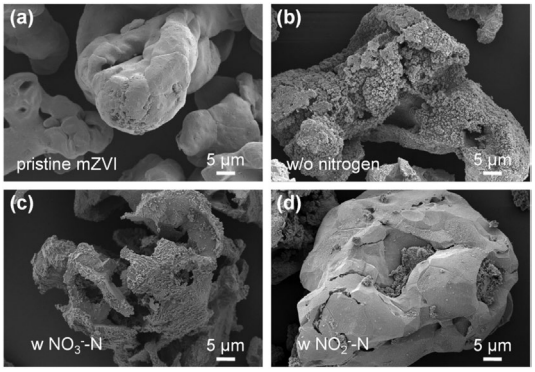


Fig. 4. SEM of mZVI before and after reaction at pH 3.5. (a) Pristine mZVI, (b) without nitrogen, (c) with NO_3^--N, (d) with NO_2^--N.

in the amounts of organic contaminants removed per unit mass of dissolved iron. To further characterize electron donor efficiency, the concept of electron efficiency (EE) was applied (Eq. 1) [34]. N_o represents electrons for organic contaminants removal (determined by COD removal). N_{Fe} denotes electrons from mZVI corrosion (quantified *via* T_{Fe}) (Text S10 in Supporting information). NO_3^--N decreased EE by 0.3 %–17.8 % across different organic contaminants (Fig. 3f). This suggests that while NO_3^--N promoted iron dissolution and particle corrosion, as visually confirmed by significant fragmentation of residual mZVI particles in SEM images (Fig. 4), it concurrently reduced the electron efficiency for organic contaminant removal [2]. Ultimately, elevated T_{Fe} cannot offset NO_3^--N-induced electron competition, wherein NO_3^--N preferentially captures the electrons released by mZVI and inhibits the transformation from O_2 to ROS, blocking the Fenton oxidation pathway.

$$EE = N_o/N_{Fe} \times 100\% \quad (1)$$

The accelerated iron dissolution by NO_3^--N, however, does not translate to improved organic contaminants removal. This discrepancy necessitates an investigation into ROS dynamics under NO_3^--N interference. To clarify the inhibition mechanism of ROS generation in the mZVI/O_2 process from NO_3^--N *via* electron competition, H_2O_2 quantification, EPR analysis, radical scavenging assays, and chemical probe tests were used for systematic validation. Theoretically, the reaction of Fe^0 and O_2 can produce H_2O_2 [11], but concurrent Fenton-driven H_2O_2 consumption results in dynamic fluctuations of H_2O_2 concentrations between 40.7–54.9 μmol/L (mean concentration: 43.2 μmol/L). Increasing NO_3^--N dosage progressively lowers equilibrium H_2O_2 levels, exemplified by a reduction to 10.2–32.9 μmol/L (mean concentration: 20.0 μmol/L) at 600 mg/L NO_3^--N (Fig. 5a). EPR was used to characterize ROS because 5,5-dimethyl-1-pyrroline-*N*-oxide (DMPO) reacts specifically with •OH to form DMPO-OH [35]. The presence of a typically quartet line of DMPO-OH ($\alpha^N = \alpha^H = 14.9$ G, 1:2:2:1) in Fig. 5b confirms the generation of •OH in the process [27]. NO_3^--N addition weakened the DMPO-OH adduct peak intensity, suggesting that NO_3^--N inhibits the cascade pathway of O_2 activation to produce H_2O_2 and •OH by competing for electrons.

Radical scavenging experiments verified the dominant role of •OH in the mZVI/O_2 process and the inhibitory effect of NO_3^--N on its generation. *Tert*–butyl alcohol (TBA) was used as a radical scavenging reagent to selectively screen •OH (k(•OH, TBA) = 6.0×10^8 L mol^{-1} s^{-1}) [36]. The presence of TBA decreased PE removal by 41.9 % (from 56.5 % to 14.6 %) without NO_3^--N and by 30.4 % (from 36.8 % to 6.4 %) with NO_3^--N (Fig. 5c). This confirms that NO_3^--N not only reduces •OH content but may also diminish secondary oxidation pathways (*e.g.*, direct surface oxidation). BA hydroxylation is an effective method for •OH quantification *via* H-abstraction producing characteristic products (Fig. 5d) [37]. Figs. 5e and f show the rapid hydroxylation of BA to 4-hydroxybenzoic acid (4-HBA) (35.6 μmol/L) and further oxidation to produce 3,4-dihydroxybenzoic acid (3,4-DHBA) (78.6 μmol/L) without NO_3^--N, indicating that the mZVI/O_2 process can continuously produce •OH and have the ability to oxidize organic contaminants in a multistep process. In contrast, the addition of NO_3^--N resulted in slower BA degradation, a lower rate of 4-HBA production, and a decrease in the accumulation of 3,4-DHBA to 56.9 μmol/L, further indicating that NO_3^--N weakened the degradation efficiency of the mZVI/O_2 process for organic contaminants by inhibiting the production of •OH.

Overall, NO_3^--N significantly regulates ROS generation and organic contaminants removal in the mZVI/O_2 process through electron competition. By competing with O_2 for electrons released during mZVI corrosion, NO_3^--N markedly suppresses the oxygen

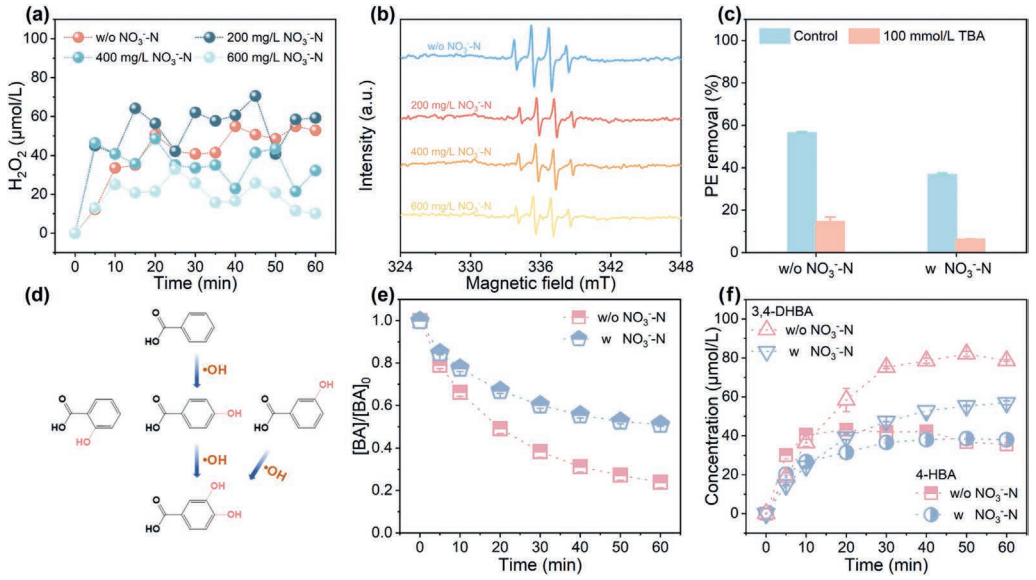


Fig. 5. (a) H_2O_2 generation, (b) EPR analysis for radicals, (c) TBA inhibition on PE removal, (d) hydroxylated products pathway, (e) and (f) BA as chemical probe for analyzing hydroxylation products.

activation cascade. This leads to reduced generation intensity of the critical oxidant •OH, thereby inhibiting multi-step oxidation processes and limiting the oxidation of organic contaminants. Combined analysis of rules of iron dissolution and ROS generation, NO_3^--N has a dual role in the mZVI/O_2 process: (1) As an electron acceptor enhancing Fe° corrosion, increasing T_{Fe} by 17.5 %–65.7 %; (2) Inhibiting the cascade pathway of O_2 activation to produce H_2O_2 and thus •OH by competing for electrons, which results in a decrease of COD removal efficiency per unit of iron consumed of up to 57.9 %.

The transformation of NO_3^--N is dominated by the direct reduction to NH_4^+-N as the dominant pathway in the mZVI/O_2 process [38]. It has been shown that NO_3^--N is preferentially reduced to NH_4^+-N by H^+-driven electron transfer through the surface of mZVI, and the TN decreased slightly after 30 min of reaction, with NH_4^+-N accounting for >98.2 % of the reduction products (Fig. 6a). The production of minor NO_2^--N (0.2 mg/L) and the decrease in TN suggest the existence of an indirect reduction pathway: a little NO_3^--N can be further transformed to NH_4^+-N and N_2 *via* the NO_2^--N intermediate state. The addition of NO_2^--N in the control experiment resulted in 100.0 % conversion, 53.0 % TN removal and 40.8 % product NH_4^+-N selection (Fig. 6b) [38]. It is further demonstrated that in the mZVI/O_2 process, most of NO_3^--N can be directly reduced into NH_4^+-N, and a little NO_3^--N will be reduced to NO_2^--N first through an indirect reduction pathway and then converted to NH_4^+-N or N_2 (Text S2) [39]. Significantly, NH_4^+-N is chemically inert in this process and neither affects the removal of organic contaminants nor participates in redox reactions (Figs. 2a and 6b).

The conversion efficiency of NO_3^--N is significantly regulated by pH and organic contaminants species (Fig. 6c and Fig. S12 in Supporting information), independent of the initial NO_3^--N concentration (Fig. S13 in Supporting information). The conversion of NO_3^--N in acidic conditions (pH 2.0–3.0) is 61.0 %–70.2 % within 60 min by accelerating the Fe° corrosion and enhancing the H^+ supply. When the pH increases, it leads to a slowing down of Fe° corrosion and a gradual decrease in the conversion rate [40,41]. In addition, the electron demand characteristics of coexisting organic contaminants can affect the conversion rate of NO_3^--N. However, the NO_3^--N reduction pathway cannot be altered regardless of changing environmental conditions, and NH_4^+-N is always

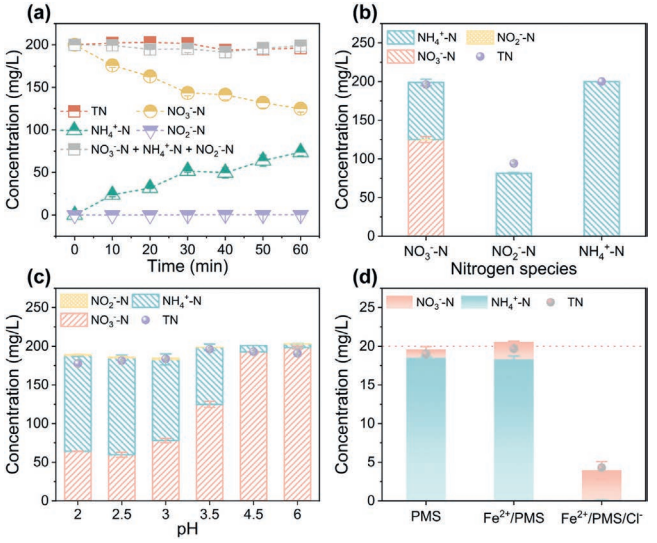


Fig. 6. Conversion of nitrogen in the mZVI/O_2 process. (a) NO_3^--N transformations, (b) transformation of different nitrogen species, (c) effect of pH on NO_3^--N conversion in the mZVI/O_2 process, (d) oxidation of NH_4^+-N by peroxymonosulfate (PMS) systems.

stabilized as the end product. Consequently, in the mZVI/O_2 process, NO_3^--N is predominantly converted to NH_4^+-N *via* a direct 8-electron reduction pathway, with the presence of the NH_4^+-N product exhibiting virtually no adverse impact on treatment efficacy.

NO_3^--N addition promotes T_{Fe} dissolutionin in the mZVI/O_2 process and is essentially in the form of Fe(II) (Fig. S14 in Supporting information). Therefore, the residual Fe(II) from the mZVI/O_2 process was coupled with extra added oxidation to construct the subsequent Fenton/Fenton-like oxidation process to deeply oxidize organic contaminants [42]. Considering the potential oxidation of NH_4^+-N by ROS generated in these Fenton/Fenton-like processes, where such oxidation may impact contaminant degradation and nitrogen resource recovery, the study systematically evaluated the NH_4^+-N oxidation capabilities of four Fenton or Fenton-like pro-

cesses. In the conventional Fenton system (Fe(II)/H_2O_2) [43], both H_2O_2 and its activated product •OH (2.7 V *vs.* NHE) exhibited negligible oxidation of NH_4^+-N under acidic conditions due to extremely slow reaction kinetics (Fig. S15a in Supporting information). It is consistent with Figs. 2a and 6b that the presence of NH_4^+-N do not affect the mZVI/O_2 process. Within the persulfate activation systems (Fe(II)/PS) [44], peroxydisulfate (PDS) and PMS activated by Fe(II) can generate $SO_4^{\bullet-}$ (2.5-3.1 V *vs* NHE), Fe(IV) (1.3-2.0 V *vs.* NHE), and •OH (Fig. 6d and Fig. S15b in Supporting information) [45,46]. These ROS struggled to oxidize positively charged NH_4^+-N owing to their electrophilic attack mechanisms. However, PMS itself slowly oxidized NH_4^+-N *via* a non-radical pathway. The peracetic acid (PAA) system (Fe(II)/PAA) primarily produced Organic Radicals (RO• 1.5–2.3 V *vs.* NHE), Fe(IV), and •OH, all displaying minimal oxidation efficiency toward NH_4^+-N (Fig. S15c in Supporting information) [47]. Collectively, although •OH, $SO_4^{\bullet-}$, Fe(IV), and RO• exhibit high redox potentials, their reaction mechanisms predominantly rely on electrophilic attack (Table S1 in Supporting information) [48,49]. The nitrogen atom in NH_4^+-N is positively charged with low electron density, exhibiting electron-deficient properties which make it resistant to oxidation by electrophilic radicals.

Considering the high salinity characteristics of some industrial organic wastewater, chloride ions (Cl^-) were introduced into the system to explore the effects on the nitrogen transformation pathways and reaction kinetics under saline conditions. The results showed that the Fe(II)/PMS/Cl^- system could completely oxidize of NH_4^+-N, and most of the NH_4^+-N was transformed to N_2. This phenomenon was mainly attributed to the action of reactive chlorine radicals (*e.g.*, ClO•, Cl•) [50]. Despite the relatively lower redox potentials of chlorine radicals (*e.g.*, Cl•: 2.4 V; ClO•: 1.5–1.8 V *vs.* NHE), they exhibit enhanced substrate-specific oxidative capacity compared to conventional radicals [51]. The reaction mechanisms of these chlorine-derived radicals predominantly involve nucleophilic attack, which enables efficient oxidation of NH_4^+-N by targeting its electron-deficient nitrogen atom and weakening N-H bonds [52]. Accordingly, the nitrogen conversion pathway in the mZVI/O_2 process is proposed: NO_3^--N competes with O_2 for the electrons released from Fe^0, and is directly reduced to NH_4^+-N through a one-step 8-electron pathway. NH_4^+-N is difficult to be oxidized not only by •OH generated in Fenton system, but also by $SO_4^{\bullet-}$, RO• or Fe(IV) from other Fenton-like systems. However, ClO•, Cl• and other reactive chlorine radicals can effectively oxidize it to N_2 or NO_3^--N (Fig. 7).

Based on the previously established electron efficiency (EE) concept (Eq. 1), this study further defines a modified electron efficiency (EE_N) to explicitly account for electrons consumed in NO_3^--N reduction (Eq. 2). EE_N considers both N_o and N_n (electrons required for NO_3^--N reduction) as an efficient use of electrons (Text S10). The results demonstrate that the addition of NO_3^--N can increase the EE_N (increased by 8.2 %–53.8 %), both in the case of treating different organic contaminants (Fig. 8a). It has been shown that NO_3^--N enhances the effective utilization of iron electrons and reduces the generation of side reactions [22], which in turn may enhance the overall efficiency of wastewater treatment in the mZVI/O_2 process.

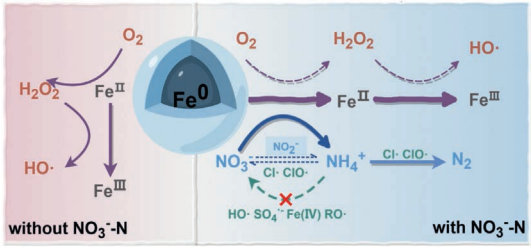


Fig. 7. Inorganic nitrogen transformation pathways in the mZVI-based process.

$$EE_N = (N_n + N_o)/N_{Fe} \times 100\,\% \quad (2)$$

Based on the characteristics that after degradation of organic contaminants and reduction of NO_3^--N by the mZVI/O_2 process: (1) Excess Fe(II) in the system is underutilized, (2) NO_3^--N can be converted to NH_4^+-N directionally, (3) NH_4^+-N is difficult to be oxidized by •OH, (4) NO_3^--N enhances the effective utilization of iron electrons. The two-stage gradient oxidation process of mZVI/O_2-Fenton has been proposed (Fig. 1b). In the 1st stage, NO_3^--N is used to promote Fe° corrosion to realize the pre-oxidation of high concentration of organic contaminants and the initial utilization of iron electrons to convert NO_3^--N to NH_4^+-N directionally. At the same time, a large amount of Fe(II) is released. In the 2nd stage, H_2O_2 is added to produce •OH *via* Fenton reaction to strengthen organic contaminant oxidation and achieve further utilization of iron electrons. The mZVI/O_2-Fenton two-stage gradient oxidation process is used to treat high-concentration NO_3^--N-contained organic wastewater, synergistically realizing highly efficient removal of organic contaminants and targeted recovery of nitrogen. It improves wastewater treatment efficiency and reduces wastewater treatment operating costs [53].

Through adjusting factors such as pH, iron dosage [39], and reaction time, the 1st stage achieves 93.1 % NO_3^--N reduction efficiency with nearly 100 % NH_4^+-N selectivity under optimal conditions (Fig. 8b). More than 91.0 % COD removal was achieved in the two-stage gradient oxidation process for treatment of organic wastewater with high concentration of organic contaminants (COD_0 2000 mg/L, Fig. 8c). Surprisingly, COD removal was better in the presence of NO_3^--N. This is the opposite of the removal effect in the 1st stage. Furthermore, the NO_3^--N conversion rate of 76.8 % with 72.7 % NH_4^+-N selectivity was achieved, demonstrating significant potential for nitrogen resource recovery (Fig. 8d). Acute toxicity test with luminescent bacteria revealed that the mZVI/O_2-Fenton two-stage gradient oxidation process significantly reduces toxicity when NO_3^--N is present (a more significant decrease in IR value) (Fig. S17, Table S2 in Supporting information) [54,55]. To evaluate the potential application of the process in actual wastewater treatment, four organic industrial wastewaters containing high concentrations of NO_3^--N (including paint wastewater, primary explosive wastewater, tetrazene wastewater and pharmaceutical wastewater) were selected for treatment experiments (Table S3 in Supporting information). The results demonstrated significant organic contaminant removal coupled with effective nitrogen transformation across all wastewaters after two-stage gradient oxidation treatment with mZVI/O_2-Fenton, despite variations in treatment efficiency among the different types. The COD removal rate was stable between 79.8 % and 93.7 % for all four wastewaters, with conversion of NO_3^--N and selectivity of NH_4^+-N higher than 64.7 % (Figs. 8e and f, and Fig. S18 in Supporting information). In addition, UV–vis was used to monitor the degradation of pollutants before and after wastewater treatment (Fig. S19 in Supporting information) [53]. The results further confirmed that the mZVI/O_2-Fenton two-stage gradient oxidation process has significant degradation and detoxification effects on organic industrial wastewater with high NO_3^--N. The 8-h continuous flow experiment confirmed the long-term operational stability of the process (Text S11 in Supporting information). For paint wastewater containing high concentrations of NO_3^--N, the effluent COD removal remained consistently above 88.1 %, with ammonia nitrogen selectivity exceeding 69.9 % (Fig. S20 in Supporting information). The mZVI/O_2-Fenton two-stage gradient oxidation process takes advantage of the high electron utilization of NO_3^--N and synergizes the directed NO_3^--N

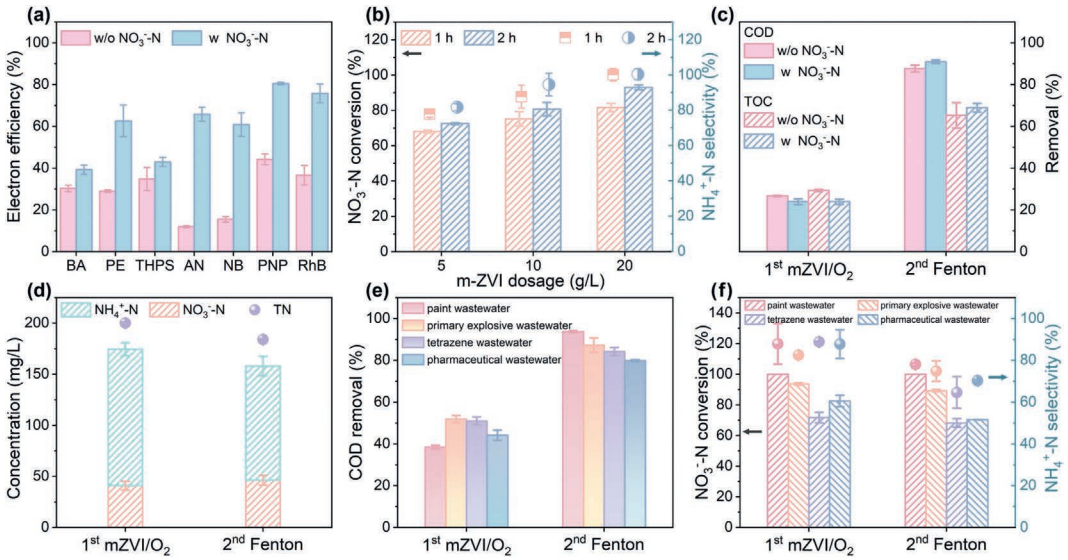


Fig. 8. (a) Iron electron utilization in different organic contaminants, (b) NO_3^--N conversion and NH_4^+-N selection with different iron dosages, (c) and (e) organic contaminants removal by two-stage gradient oxidation process, (d) and (f) NO_3^--N transformation in a two-stage gradient oxidation process.

transformation and the high efficiency removal of organic contaminants. It provides an innovative solution based on efficient treatment and nitrogen recovery for refractory organic wastewater with high concentration of NO_3^--N.

This study reveals the dual regulatory mechanism of NO_3^--N in the mZVI/O_2 process. NO_3^--N acts as an electron acceptor to promote Fe° corrosion, increasing iron ion dissolution by 17.5 %–65.7 % under various pH conditions compared to the system without NO_3^--N. And meanwhile, it inhibits ROS generation pathways through electron competition, thereby reducing organic contaminants removal efficiency. Analysis of nitrogen transformation pathways demonstrates that NO_3^--N is predominantly converted to NH_4^+-N *via* a direct 8-electron reduction pathway, with the resultant NH_4^+-N exhibiting chemical inertness in the mZVI/O_2 process. Based on these findings, a novel mZVI/O_2-Fenton two-stage gradient oxidation process was developed: 1st stage leverages the corrosion-enhancing effect of NO_3^--N to achieve targeted NH_4^+-N reduction (76.8 % NO_3^--N conversion, 72.7 % NH_4^+-N selectivity), while 2nd stage employs the Fenton reaction to efficiently degrade organic contaminants, resulting in 91.0 % removal of COD. Critically, NO_3^--N addition promotes iron dissolution through direct redox reactions with mZVI, elevating effective iron electron utilization efficiency (EE_N increased by 8.2 %–53.8 %) and subsequently liberating more Fe(II) for 2nd stage. The process achieves >79.8 % COD removal for four actual wastewaters (including paint wastewater, primary explosive wastewater, tetrazene wastewater and pharmaceutical wastewater), with NO_3^--N conversion rates and NH_4^+-N selectivity higher than 64.7 %, demonstrating its application potential for treating a variety of refractory industrial wastewaters. Therefore, the corrosion-promoting effect of NO_3-N for mZVI was utilized to overcome the bottleneck of electron competition in the treatment of nitrogen-contained refractory organic wastewater by the mZVI/O_2 process, and meanwhile, the efficient degradation of organic contaminants and simultaneous recovery of nitrogen resources were realized by the mZVI/O_2-Fenton two-stage gradient oxidation process.

Declaration of competing interest

The authors declare that they have no known competing financial interests or personal relationships that could have appeared to influence the work reported in this paper.

CRediT authorship contribution statement

Yan Zhang: Writing – review & editing, Writing – original draft, Visualization, Investigation, Formal analysis, Data curation. **Shuo Chen:** Visualization, Formal analysis. **Huihui Peng:** Visualization, Formal analysis. **Ankang Wang:** Formal analysis. **Yiming Sun:** Formal analysis. **Chenying Zhou:** Visualization, Formal analysis. **Shuang Meng:** Visualization, Formal analysis. **Chuanshu He:** Supervision. **Peng Zhou:** Writing – review & editing, Writing – original draft, Visualization, Project administration, Investigation, Formal analysis, Data curation. **Bo Lai:** Writing – review & editing, Supervision, Project administration, Funding acquisition.

Acknowledgments

This research was supported financially by National Natural Science Foundation of China (No. U24A20561) and Sichuan Science and Technology Program (No. 2024NSFTD0014).

Supplementary materials

Supplementary material associated with this article can be found, in the online version, at doi:10.1016/j.cclet.2025.112209.

References

[1] P. Jiang, T. Zhou, J. Bai, et al., Water Res. 235 (2023) 119914.
[2] X. Wang, J. Xin, M. Yuan, F. Zhao, Water Res. 183 (2020) 116060.
[3] M. Farghali, Z. Chen, A.I. Osman, et al., Environ. Chem. Lett. 22 (2024) 2699–2751.
[4] X. Huang, S. Liu, G. Liu, et al., Appl. Catal. B 323 (2023) 122134.
[5] Y. Yuan, Z. Zhou, X. Zhang, et al., Chin. Chem. Lett. 34 (2023) 107932.
[6] Z. Jiang, L. Lv, W. Zhang, et al., Water Res. 45 (2011) 2191–2198.
[7] K. Wei, Y. Wan, M. Liao, et al., Water Res. 218 (2022) 118453.
[8] J. Yu, X. Hou, X. Hu, et al., Appl. Catal. B Energy 256 (2019) 117876.
[9] L.J. Matheson, P.G. Tratnyek, Environ. Sci. Technol. 28 (1994) 2045–2053.
[10] X. Zhou, X. Li, Y. Xiang, et al., Chin. Chem. Lett. 36 (2025) 110664.
[11] X. Guan, Y. Sun, H. Qin, et al., Water Res. 75 (2015) 224–248.
[12] J. Wu, J. Zhao, J. Hou, et al., Environ. Sci. Technol. 53 (2019) 8105–8114.
[13] J. Xie, Y. Zheng, Q. Zhang, et al., Appl. Catal. B: Environ. Energy 320 (2023) 121935.
[14] Z. Xiong, B. Lai, Y. Yuan, et al., Chem. Eng. J. 302 (2016) 137–145.
[15] Z. Xiong, B. Lai, P. Yang, et al., J. Hazard. Mater. 297 (2015) 261–268.
[16] Y. Wang, L. Li, X. Guo, et al., Water Res. 268 (2025) 122648.
[17] F. Fu, D.D. Dionysiou, H. Liu, J. Hazard. Mater. 267 (2014) 194–205.
[18] J.M. Rodriguez-Maroto, F. Garcia-Herruzo, A. Garcia-Rubio, et al., Chemosphere 74 (2009) 804–809.

[19] T. Suzuki, M. Moribe, Y. Oyama, M. Niinae, Chem. Eng. J. 183 (2012) 271–277.
[20] Q. Lu, S.-W. Jeen, L. Gui, R.W. Gillham, Water Res. 112 (2017) 48–57.
[21] H. Liu, Q. Wang, C. Wang, X. Li, Chem. Eng. J. 215-216 (2013) 90–95.
[22] H. Qin, X. Guan, P.G. Tratnyek, Environ. Sci. Technol. 53 (2019) 9744–9754.
[23] J. Wang, X. Li, S. Shen, et al., ACS Catal 13 (2023) 8783–8791.
[24] Y.H. Huang, T.C. Zhang, P.J. Shea, S.D. Comfort, J. Environ. Eng. 140 (2014) 04014029.
[25] Y. Sun, J. Li, T. Huang, X. Guan, Water Res. 100 (2016) 277–295.
[26] K. Ritter, M.S. Odziemkowski, R. Simpgraga, et al., J. Contam. Hydrol. 65 (2003) 121–136.
[27] C. Qin, J. Zhang, C. Zhang, et al., Environ. Sci. Technol. 55 (2021) 6828–6837.
[28] C. Le, J.H. Wu, S.B. Deng, et al., Water Sci. Technol. 63 (2011) 1485–1490.
[29] J.A. Donadelli, L. Carlos, A. Arques, F.S. García Einschlag, Appl. Catal. B: Environ. Energy 231 (2018) 51–61.
[30] M.P. Rayaroth, C.S. Lee, U.K. Aravind, et al., Chem. Eng. J. 315 (2017) 426–436.
[31] Y. Xiang, Y. Liu, B. Cong, et al., Water Res. 267 (2024) 122494.
[32] C. Xue, Y. Peng, A. Chen, et al., J. Colloid Interface Sci. 582 (2021) 22–29.
[33] W. Yin, J. Wu, P. Li, et al., Chem. Eng. J. 184 (2012) 198–204.
[34] P. Fan, L. Li, Y. Sun, et al., Water Res. 159 (2019) 375–384.
[35] S. Pei, S. You, J. Ma, et al., Environ. Sci. Technol. 54 (2020) 13333–13343.
[36] P. Zhou, Y. Yang, W. Ren, et al., Appl. Catal. B 319 (2022) 121916.
[37] Y. Sun, P. Zhou, P. Zhang, et al., Chem. Eng. J. 450 (2022) 138423.
[38] M.J. Alowitz, M.M. Scherer, Environ. Sci. Technol. 36 (2002) 299–306.
[39] Y. Zhang, G.B. Douglas, L. Pu, et al., Sci. Total Environ. 598 (2017) 1140–1150.
[40] Y.H. Huang, T.C. Zhang, Water Res. 38 (2004) 2631–2642.
[41] H. Hu, Y. Bai, C. Zhou, et al., Environ. Sci. Technol. 58 (2024) 9804–9814.
[42] Z. Yang, C. Shan, Y. Mei, et al., Chem. Eng. J. 334 (2018) 2255–2263.
[43] L. Huang, L. Li, W. Dong, et al., Environ. Sci. Technol. 42 (2008) 8070–8075.
[44] Y. Gao, Y. Luo, Z. Pan, et al., Water Res. 249 (2024) 120967.
[45] Z. Wang, J. Jiang, S. Pang, et al., Environ. Sci. Technol. 52 (2018) 11276–11284.
[46] P. Wang, H. Zhang, Z. Wu, et al., Chin. Chem. Lett. 34 (2023) 108722.
[47] J. Kim, T. Zhang, W. Liu, et al., Environ. Sci. Technol. 53 (2019) 13312–13322.
[48] Y. Tong, X. Wang, Y. Zhang, et al., Water Res. 272 (2025) 122917.
[49] X. Fan, Y. Zhou, G. Zhang, et al., Appl. Catal. B 244 (2019) 396–406.
[50] Q. Guo, Z. Xu, W. Jin, Sep. Purif. Technol. 342 (2024) 127024.
[51] D. Song, B. Qiao, X. Wang, et al., Environ. Sci. Technol. 57 (2023) 9416–9425.
[52] M. Kurban, Y. Zhang, Y. Wang, et al., J. Environ. Chem. Eng. 12 (2024) 112630.
[53] Y. Yuan, B. Lai, P. Yang, Y. Zhou, J. Taiwan Inst. Chem. Eng. 65 (2016) 286–294.
[54] L. Hu, M. Rossetti, J.F. Bergua, et al., ACS Appl. Mater. Interfaces. 16 (2024) 30636–30647.
[55] E. Fulladosa, J.C. Murat, I. Villaescusa, Chemosphere 58 (2005) 551–557.